Published by IOP Publishing for Sissa Medialab

Received: *November 29, 2025*
Accepted: *January 19, 2026*
Published: *February 17, 2026*

17TH Topical Seminar on Innovative Particle and Radiation Detectors
Siena, Italy
15–19 September 2025

Measurements and radiation damage modelling of small-pitch 3D pixel detectors at high fluences

K. Aouadj,[a,*] **A. Morozzi**,[a] **A. Fondacci**,[b,a] **T. Croci**,[a] **D. Passeri**,[c,a] **V. Sola**,[d,e] **R.S. White**,[e] **M. Ferrero**,[e] **J. Ye**,[f,g] **G.-F. Dalla Betta**[f,g] **and F. Moscatelli**[h,a]

[a] *INFN Perugia, via A. Pascoli, Perugia, Italy*
[b] *Department of Physics, University of Perugia, via A. Pascoli, Perugia, Italy*
[c] *Department of Engineering, University of Perugia, via G. Duranti 93, Perugia, Italy*
[d] *Department of Physics, University of Torino, via P. Giuria 1, Torino, Italy*
[e] *INFN Torino, via P. Giuria 1, Torino, Italy*
[f] *Department of Industrial Engineering, University of Trento, via Sommarive 9, Trento, Italy*
[g] *TIFPA INFN, Via Sommarive 14, 38123 Trento, Italy*
[h] *CNR, Istituto Officina dei Materiali (IOM), via A. Pascoli, Perugia, Italy*

E-mail: khaoula.aouadj@pg.infn.it

Abstract: The macroscopic electrical response of small-pitch$50 \times 50\ \mu m^2$ 3D pixel sensors was investigated by comparing experimental measurements with TCAD simulations. Selected trap parameters (introduction rates and capture cross sections) of the CERN (Folkestad) model, originally developed for fluences up to $8 \times 10^{15}\ n_{eq}/cm^2$, were varied to study their impact on the simulated characteristics and to assess the sensitivity in reproducing the measured behaviour. The analysis focuses on the I-V, C-V, and charge collection efficiency (CCE) characteristics at fluences of $1 \times 10^{16}\ n_{eq}/cm^2$ and $2.5 \times 10^{16}\ n_{eq}/cm^2$. This work highlights how variations in trap parameters influence the performance of irradiated 3D sensors and supports the extension of the CERN model for 3D detectors operating at high fluence.

Keywords: Detector modelling and simulations II (electric fields, charge transport, multiplication and induction, pulse formation, electron emission, etc); Radiation damage to detector materials (solid state); Radiation-hard detectors; Solid state detectors

*Corresponding author.

© 2026 The Author(s). Published by IOP Publishing Ltd on behalf of Sissa Medialab. Original content from this work may be used under the terms of the Creative Commons Attribution 4.0 licence. Any further distribution of this work must maintain attribution to the author(s) and the title of the work, journal citation and DOI.

https://doi.org/10.1088/1748-0221/21/02/C02022

2026 JINST 21 C02022

Contents

1 **Introduction** 1

2 **Devices under test and measurement setup** 2

2.1 Device description 2

2.2 Measurements 2

3 **TCAD simulations framework** 3

4 **Results and discussion** 4

5 **Conclusions** 7

2026 JINST 21 C02022

1 Introduction

The continuous increase in luminosity foreseen at future colliders, such as the High-Luminosity Large Hadron Collider (HL-LHC), will expose tracking detectors to fluences exceeding those reached so far, approaching $2 \times 10^{16}\, n_{\mathrm{eq}}/\mathrm{cm}^2$. At such irradiation levels, conventional silicon technologies suffer from significant degradation of key performance characteristics [1], making radiation tolerance one of the central challenges in detector design. Among the proposed radiation-hard devices, 3D silicon pixel detectors [2, 3] use vertical electrodes to shorten the carrier drift path. This approach reduces charge trapping and preserves signal collection efficiency even after high levels of irradiation. This intrinsic advantage has already led to the successful integration of 3D sensors in collider experiments and motivates their use in the innermost layers of upgraded trackers [4, 5].

Within this framework, Technology Computer-Aided Design (TCAD) suite of software [6, 7] provides a powerful tool to investigate detector behavior. Radiation damage models can be included into device simulations to accurately account for their effects. Numerical simulations, therefore, provide a reliable way to predict how device performance will evolve with irradiation. However, most existing numerical models [8–13] have been calibrated only up to fluences about $10^{16} n_{\mathrm{eq}}/\mathrm{cm}^2$, so their predictive accuracy at higher fluences remains limited.

For 3D detectors, the CERN three-level bulk model (valid from −38.1°C to −31.1°C, and for fluences up to $8 \times 10^{15}\, n_{\mathrm{eq}}/\mathrm{cm}^2$) [10], an extension of the EVL [8, 14] scheme with an additional defect level to improve charge collection efficiency (CCE), has been successfully applied to $50 \times 50\ \mu\mathrm{m}^2$ 3D diodes. It reproduces I-V and CCE trends well, though it tends to overestimate the breakdown voltage [15, 16]. Its application on C-V characteristics has not been systematically investigated, apart from a previous study by Moscatelli et al. [17].

Building on this background, the present work adopts the CERN bulk model [10] as a reference framework (table 1) and critically evaluates it as a function of the fluence. The effect of trap capture cross sections and introduction rates of bulk traps has been investigated through TCAD simulations on small-pitch 3D pixel detectors, and the resulting electrical characteristics are benchmarked against experimental measurements performed at fluences up to $2.5 \times 10^{16}\, n_{\mathrm{eq}}/\mathrm{cm}^2$. This comparison aims to assess and enhance the model's ability to reproduce key macroscopic behaviors (I-V, C-V, and CCE) in irradiated 3D sensors.

Table 1. Trap parameters of the CERN bulk damage model. Energy levels are given relative to the conduction- (E_c) and valence-band (E_v) edges.

Type	Energy level	σ_e [cm^{-2}]	σ_h [cm^{-2}]	η [cm^{-1}]
Donor	$E_v + 0.48$	2×10^{-14}	1×10^{-14}	4
Acceptor	$E_c - 0.525$	5×10^{-15}	1×10^{-14}	0.75
Acceptor	$E_v + 0.90$	1×10^{-16}	1×10^{-16}	36

2 Devices under test and measurement setup

2.1 Device description

The device under study is a 50×50 µm^2 small-pitch 3D pixel detector, fabricated by Fondazione Bruno Kessler (FBK) on p-type silicon. Columnar electrodes are etched perpendicularly into the substrate from the front side by Deep Reactive Ion Etching (DRIE). The sensor has an active thickness of about 150 µm, optimized in terms of signal amplitude and sensor capacitance [18]. Each pixel contains one n$^+$ readout electrode surrounded by p$^+$ bias electrodes. The n$^+$ electrodes stop at a safety distance ~ 30 µm (gap) from the handle wafer to prevent early breakdown, while the p$^+$ electrodes penetrate into the handle wafer to allow biasing from the back side. This geometry provides a short inter-electrode distance ~ 35 µm, ensuring excellent radiation hardness [16, 18]. A schematic cross section and a layout of the device are shown in figure 1.

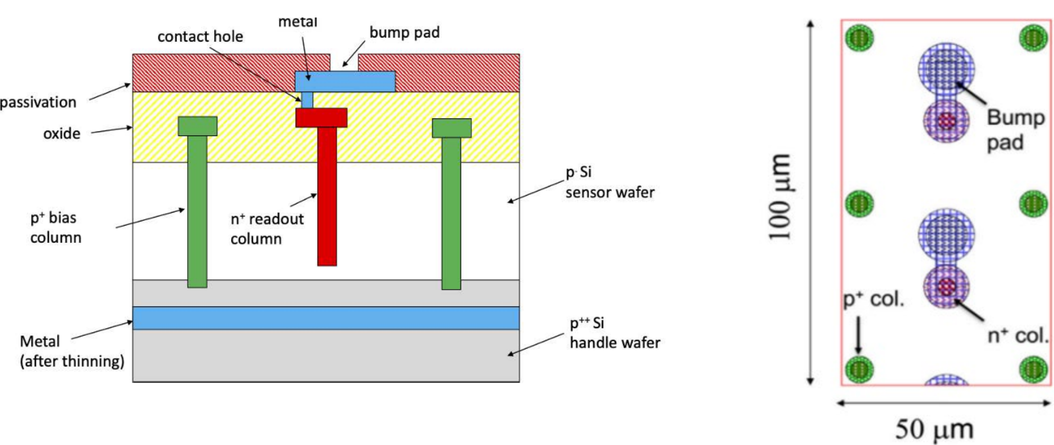

Figure 1. Device under study: left, schematic cross section; right, top-view layout of a 50×100 µm^2 region corresponding to two adjacent 50×50 µm^2 unit cells. Reproduced from [18]. CC BY 4.0.

2.2 Measurements

Neutron irradiation was performed at the TRIGA Mark II reactor at the Jozef Stefan Institute (Ljubljana, Slovenia) with the fluences of $1 \times 10^{16}\, n_{\mathrm{eq}}/\mathrm{cm}^2$ and $2.5 \times 10^{16}\, n_{\mathrm{eq}}/\mathrm{cm}^2$. The uncertainty in the neutron fluences is within 10%. The sensors were cooled down to −25°C, and all the diodes were measured under the same conditions on a semiautomatic probe station with a Keithley 707A switching matrix [19], Keithley SMU 236 and 237 for I-V measurements [20], and Agilent 4284A [21] for high-frequency C-V measurements.

2026 JINST 21 C02022

Since the ultimate purpose of this work is the analysis of the leakage current, the breakdown voltage, the depletion voltage, and the CCE, we mainly focused on the I-V characteristics and C-V measurements. The depletion voltage was determined by fitting the linear region of the $(1/C^2)$ dependence as a function of the applied reverse bias and the region where the capacitance becomes constant at high reverse bias. The intersection point between these two fits was taken as the depletion voltage. For the CCE, experimental measurements reported in ref. [22] were used to compare to simulation.

At fluence $1 \times 10^{16}\, n_{\text{eq}}/\text{cm}^2$, the I-V measurements show a breakdown voltage in the range of 300–320 V, with a noticeable increase in leakage current after depletion, which happens near 170 V. The depletion voltages extracted are in the range of 85–90 V for 500 Hz frequency and 70–85 V for 1 kHz.

At the higher fluence $2.5 \times 10^{16}\, n_{\text{eq}}/\text{cm}^2$, all the diodes have a similar breakdown voltage around 300 V, but with a larger leakage current, consistent with radiation-induced damage. The depletion voltages increase with the irradiation, reaching values above 120 V for the diodes measured, with a noticeable dependence on the frequency. The experimental results are shown in figure 2.

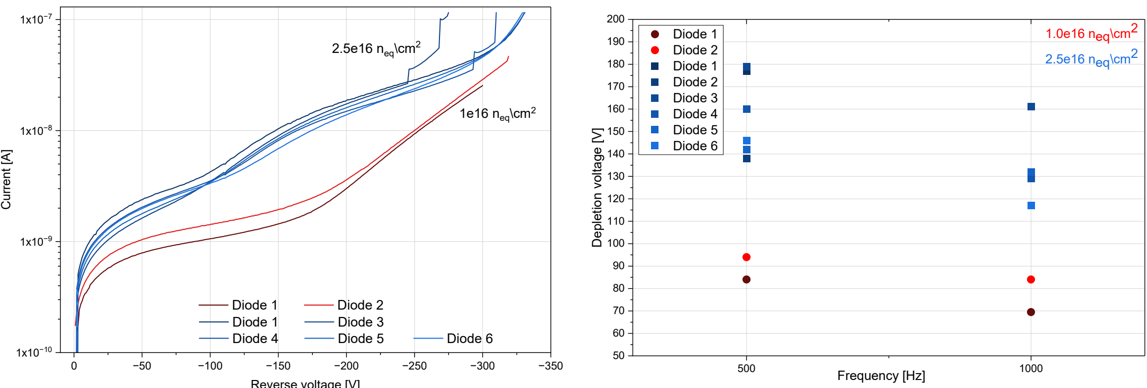

Figure 2. Left: measured I-V characteristics of different 3D diodes irradiated at two fluences, $1 \times 10^{16}\, n_{\text{eq}}/\text{cm}^2$ (red) and $2.5 \times 10^{16}\, n_{\text{eq}}/\text{cm}^2$ (blue) Right: corresponding depletion voltage extracted from C-V measurements at 500 Hz and 1 kHz for the same fluences.

3 TCAD simulations framework

To explore how trap parameters affect the macroscopic behavior of the 3D diodes, TCAD simulations were performed using Synopsys Sentaurus ® on three-dimensional domains (figure 3). It is possible to take advantage of the cell symmetry to reduce the number of grid points and the overall simulation time via the following configurations:

- One quarter of the pixel shown in figure 3(a): the red region on the front side represents the n^+ readout electrode, while the p^+ bias electrode is located in the opposite corner and in the bottom p^{++} handle wafer, with an active thickness of 150 µm and electrodes nominal radius of $\sim$ 3 µm.

- For the CCE studies, a transversal slice of 1 µm thick taken at half the device depth was simulated (figure 3(b)), following the same approach as in [15], considering a hit from a Minimum Ionizing Particle (MIP) at different points within the active area.

2026 JINST 21 C02022

Simulations included standard physical models such as doping-dependent Shockley-Read-Hall generation/recombination and mobility, high-field saturation, and Van Overstraeten-De Man for ionization impact. Radiation damage was modeled using the CERN three-level bulk damage model at −38°C, the temperature at which the model was validated. The leakage current was scaled to −25°C using the Chilingarov formula [23] for comparison with the measured results.
Starting from reference values reported in table 1, trap introduction rates (η) and capture cross sections (σ) were systematically varied to evaluate their influence on the simulated macroscopic behavior of the 3D devices. The results are discussed in section 4.

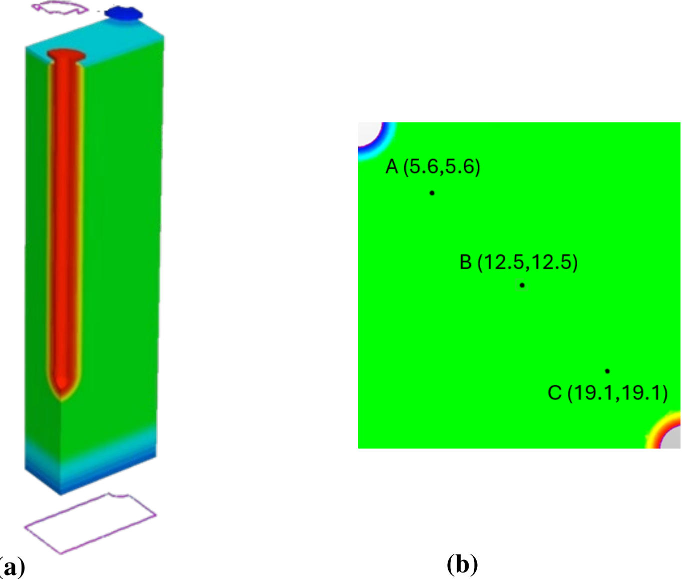

Figure 3. (a) Geometry used for I-V and C-V TCAD simulation; (b) Slice used for CCE simulations with MIP hit points.

4 Results and discussion

The TCAD simulation results of varying parameters of the deep acceptor level ($E_c - 0.525$) and donor level ($E_v + 0.48$) on the macroscopic behavior (leakage current, breakdown voltage, depletion voltage, and CCE) are shown in figures 4–7.

As illustrated in figure 4, increasing the acceptor introduction rate η_{acc} slightly reduces the leakage current below ~50 V, followed by a clear rise at higher bias for both fluences. The breakdown voltage shifts to lower values for $1 \times 10^{16}\, n_{\text{eq}}/\text{cm}^2$ and to higher ones at $2.5 \times 10^{16}\, n_{\text{eq}}/\text{cm}^2$, while the depletion voltage increases in both cases. The CCE decreases up to around ~120 V and then increases at higher bias, with a more pronounced effect at the lower fluence. Conversely, increasing the donor introduction rate η_{don} (figure 5) leads to a moderate rise in the leakage current for $1 \times 10^{16}\, n_{\text{eq}}/\text{cm}^2$, while at the higher fluence the variation shows multiple regimes across bias. The breakdown voltage decreases for the lower fluence and increases for the higher one, while the depletion voltage falls in both. The CCE remains roughly constant up to ~75 V before decreasing.

2026 JINST 21 C02022

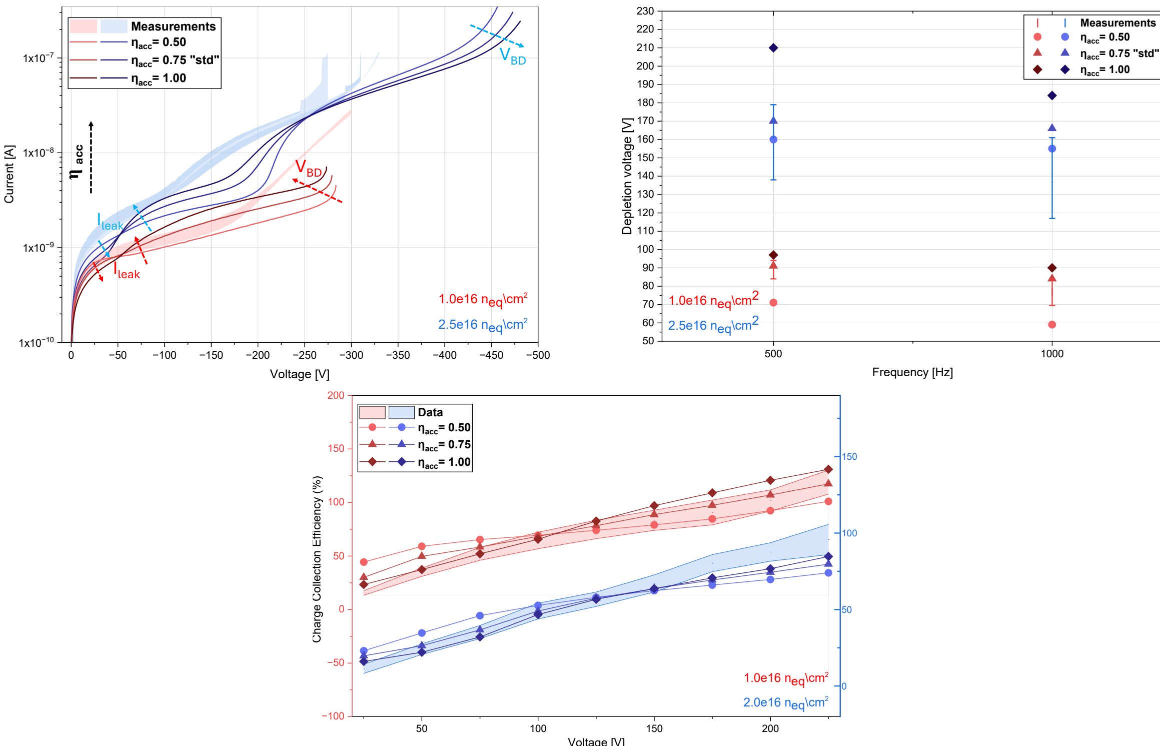

Figure 4. Effect of the acceptor introduction rate on simulated I-V curves (top left), extracted depletion voltage from simulated C-V (top right), and simulated CCE vs. bias (bottom) at $1 \times 10^{16}\, n_{\mathrm{eq}}/\mathrm{cm}^2$ (red) and $2.5 \times 10^{16}\, n_{\mathrm{eq}}/\mathrm{cm}^2$ (blue).

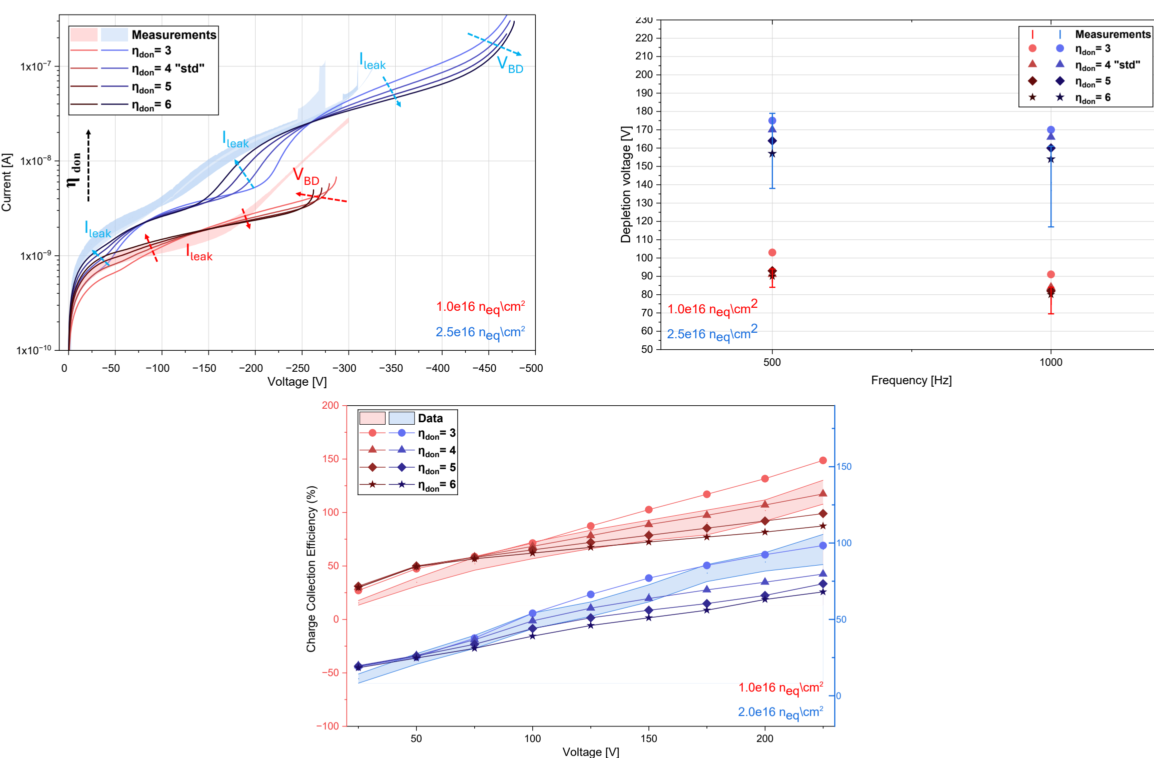

Figure 5. Effect of the donor introduction rate on simulated I-V curves (top left), extracted depletion voltage from simulated C-V (top right), and simulated CCE vs. bias (bottom) at $1 \times 10^{16}\, n_{\mathrm{eq}}/\mathrm{cm}^2$ (red) and $2.5 \times 10^{16}\, n_{\mathrm{eq}}/\mathrm{cm}^2$ (blue).

2026 JINST 21 C02022

The results in figures 6–7 show that varying the capture cross sections of the acceptor and donor traps (σ_{acc} and σ_{don}) produces distinct, fluence-dependent responses. Increasing σ_{acc} affects the leakage current only above ~50 V, producing a pronounced rise at $1 \times 10^{16}\, n_{\text{eq}}/\text{cm}^2$, while at $2.5 \times 10^{16}\, n_{\text{eq}}/\text{cm}^2$ the current above ~250 V is invariant of σ_{acc}; the breakdown voltage remains almost constant and the depletion voltage shows only a slight reduction with increasing σ_{acc}. For charge collection, a larger σ_{acc} mildly reduces CCE at low bias with a small recovery above ~100 V for the lower fluence. By contrast, increasing σ_{don} yields a more complex behavior: at $1 \times 10^{16}\, n_{\text{eq}}/\text{cm}^2$ the leakage current generally rises with σ_{don}, whereas at $2.5 \times 10^{16}\, n_{\text{eq}}/\text{cm}^2$ it first increases then decreases across the bias sweep, producing multiple regimes; the breakdown voltage falls at the lower fluence but increases for the higher one (with an early breakdown near ~230 V for $\sigma_{\text{don}} = 5 \times 10^{-15}$ and $1 \times 10^{-14}\text{cm}^{-2}$), the depletion voltage responds oppositely for the two fluences, and CCE degrades with larger σ_{don}, although this appears at lower bias for the higher fluence.

Overall, the results show that varying the trap introduction rates and capture cross sections significantly affects the simulated leakage current, breakdown voltage, depletion voltage, and CCE, and the trends observed are not identical for the two investigated fluences, indicating that the sensor response changes with irradiation level.

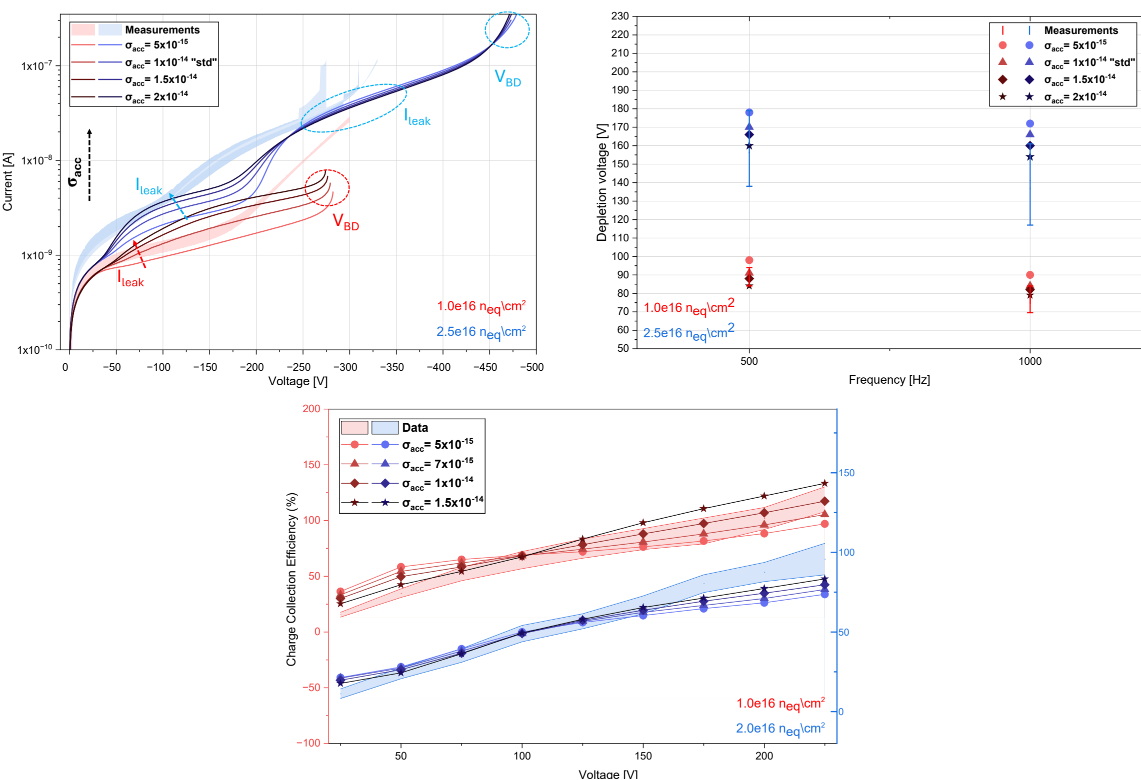

Figure 6. Effect of the acceptor capture cross section on simulated I-V curves (top left), extracted depletion voltage from simulated C-V (top right), and simulated CCE vs. bias (bottom) at $1 \times 10^{16}\, n_{\text{eq}}/\text{cm}^2$ (red) and $2.5 \times 10^{16}\, n_{\text{eq}}/\text{cm}^2$ (blue).

2026 JINST 21 C02022

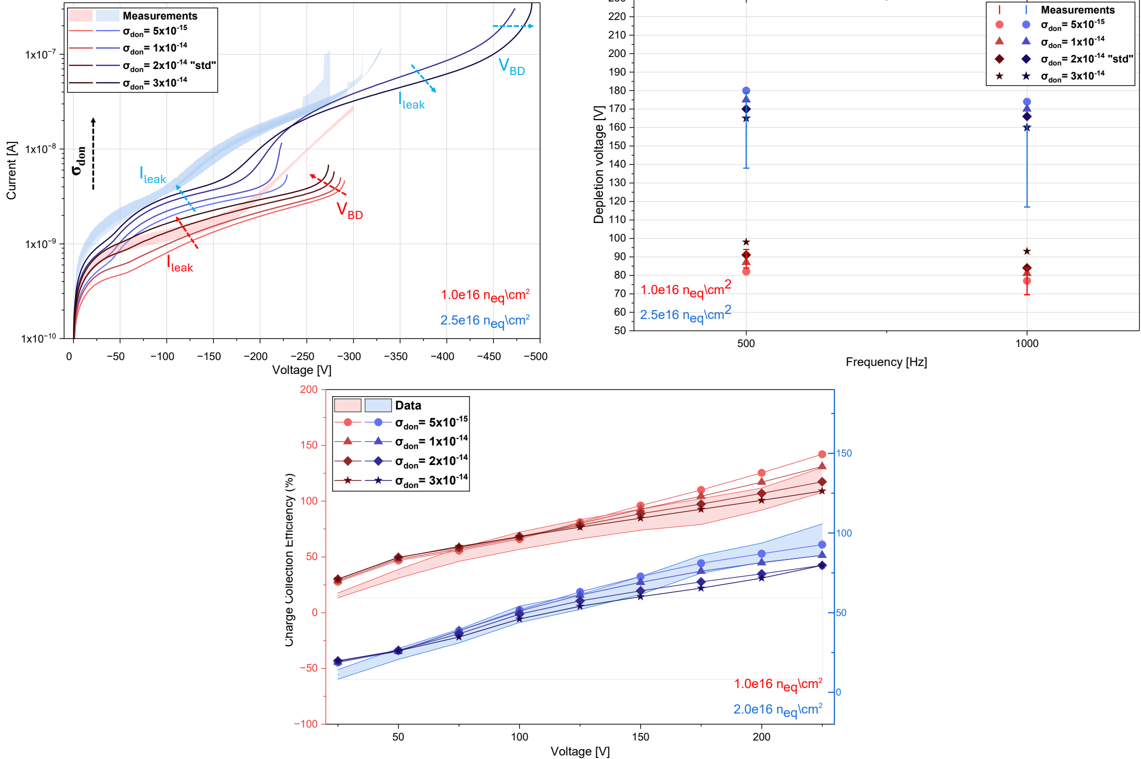

Figure 7. Effect of the donor capture cross section on simulated I-V curves (top left), extracted depletion voltage from simulated C-V (top right), and simulated CCE vs. bias (bottom) at $1 \times 10^{16}\, n_{\mathrm{eq}}/\mathrm{cm}^2$ (red) and $2.5 \times 10^{16}\, n_{\mathrm{eq}}/\mathrm{cm}^2$ (blue).

5 Conclusions

Small-pitch $50 \times 50\ \mu\mathrm{m}^2$ 3D silicon sensors irradiated with neutrons at the Jozef Stefan Institute to a fluence of $2.5 \times 10^{16}\, n_{\mathrm{eq}}/\mathrm{cm}^2$ have been electrically characterised through I-V and C-V measurements at $-25°$C.

The experimental results were compared with TCAD simulations implemented in a full three-dimensional framework using the CERN (Folkestad) radiation damage model, selected for its ability to best reproduce the observed macroscopic behavior. Since this model is originally validated only up to $8 \times 10^{15}\, n_{\mathrm{eq}}/\mathrm{cm}^2$, a systematic parametric analysis was carried out by varying trap introduction rates and capture cross sections to investigate their impact on leakage current, depletion voltage, breakdown voltage, and CCE, at the higher fluences accounted for in this paper

The study shows that the CERN model provides a solid baseline for describing the main radiation-induced effects in 3D sensors, but its direct extrapolation to higher fluences is insufficient.

The new experimental data at higher irradiation levels provide valuable guidance on the direction in which the model parameters should be adjusted, a first step towards a more accurate and predictive modelling of 3D detectors operating in extreme radiation environments, with further refinements and improved characterizations planned in future work.

2026 JINST 21 C02022

Acknowledgments

This project has received funding from the European Union's Horizon 2020 Research and Innovation Programme under GAs Nos 101004761 (AIDAinnova) and 101057511 (EURO-LABS), the PRIN MUR project 2022RK39RF 'ComonSens', and the European Union (ERC, CompleX, 101124288). Views and opinions expressed are, however, those of the authors only and do not necessarily reflect those of the European Union or the European Research Council. Neither the European Union nor the granting authority can be held responsible for them.

References

[1] M. Moll, *Displacement damage in silicon detectors for high energy physics*, *IEEE Trans. Nucl. Sci.* **65** (2018) 1561.

[2] S.I. Parker, C.J. Kenney and J. Segal, *3-D: A new architecture for solid state radiation detectors*, *Nucl. Instrum. Meth. A* **395** (1997) 328.

[3] C. Kenney, S. Parker, J. Segal and C. Storment, *Silicon detectors with 3-D electrode arrays: fabrication and initial test results*, *IEEE Trans. Nucl. Sci.* **46** (1999) 1224.

[4] D. Vázquez Furelos et al., *3D sensors for the HL-LHC*, 2017 *JINST* **12** C01026 [arXiv:1610.08889].

[5] G.-F. Dalla Betta et al., *Development of a new generation of 3D pixel sensors for HL-LHC*, *Nucl. Instrum. Meth. A* **824** (2016) 386 [arXiv:1612.00624].

[6] Silvaco Inc., *Silvaco TCAD*, https://silvaco.com/tcad/.

[7] Synopsys Inc., *Synopsys Sentaurus TCAD*, https://www.synopsys.com/.

[8] V. Eremin, E. Verbitskaya and Z. Li, *The origin of double peak electric field distribution in heavily irradiated silicon detectors*, *Nucl. Instrum. Meth. A* **476** (2002) 556.

[9] R. Eber, *Untersuchung neuartiger Sensorkonzepte und Entwicklung eines effektiven Modells der Strahlenschädigung für die Simulation hochbestrahlter Silizium-Teilchendetektoren*, Ph.D. Thesis, Karlsruher Institut für Technologie (KIT) (2013) [DOI:10.5445/IR/1000038403].

[10] Å. Folkestad et al., *Development of a silicon bulk radiation damage model for Sentaurus TCAD*, *Nucl. Instrum. Meth. A* **874** (2017) 94.

[11] J. Schwandt et al., *A new model for the TCAD simulation of the silicon damage by high fluence proton irradiation*, in the proceedings of the *2018 IEEE Nuclear Science Symposium and Medical Imaging Conference*, Sydney, NSW, Australia (2018), p. 1–3 [DOI:10.1109/NSSMIC.2018.8824412] [arXiv:1904.10234].

[12] C. Jain et al., *Modeling of neutron radiation-induced defects in silicon particle detectors*, *Semicond. Sci. Technol.* **35** (2020) 045021.

[13] D. Passeri and A. Morozzi, *TCAD Radiation Damage Model*, AIDA-2020-D7.4 (2019).

[14] V. Eremin et al., *Double peak electric field distortion in heavily irradiated silicon strip detectors*, *Nucl. Instrum. Meth. A* **535** (2004) 622.

[15] A. Boughedda et al., *Comparing different bulk radiation damage models in TCAD simulations of small-pitch 3D Si sensors*, 2021 *JINST* **16** C10006.

[16] J. Ye, A. Boughedda, D.M.S. Sultan and G.-F. Dalla Betta, *TCAD Analysis of Leakage Current and Breakdown Voltage in Small Pitch 3D Pixel Sensors*, *Sensors* **23** (2023) 4732.

2026 JINST 21 C02022

[17] F. Moscatelli et al., *TCAD modeling of bulk and surface radiation damage effects in silicon devices*, 2025 *JINST* **20** C09006.

[18] S. Terzo et al., *Novel 3D Pixel Sensors for the Upgrade of the ATLAS Inner Tracker*, *Front. in Phys.* **9** (2021) 2.

[19] Tektronix/Keithley Instruments, *Model 707a switching matrix mainframe*, `https://download.tek.com/manual/707A_901_01A.pdf` (2015).

[20] Keithley Instruments, *Models 236/237 source measure units*, `https://manualmachine.com/keithley/238/4664253-datasheet/`.

[21] Keysight/Agilent Technologies, *4284a precision lcr meter, 20 hz to 1 mhz*, `https://www.keysight.com/us/en/assets/7018-09162/data-sheets-archived/5963-5390.pdf`, (2004).

[22] R. Mendicino, M. Boscardin and G.-F. Dalla Betta, *Characterization of FBK small-pitch 3D diodes after neutron irradiation up to* $3.5 \times 10^{16}\, n_{eq}\, cm^{-2}$, 2019 *JINST* **14** C01005 [`arXiv:1810.05856`].

[23] A. Chilingarov, *Temperature dependence of the current generated in Si bulk*, 2013 *JINST* **8** P10003.